sciendo

Transactions on Aerospace Research eISSN 2545-2835, VOL. 266, NO. 1/2022, 1-17
DOI: 10.2478/tar-2022-0001

METHOD OF DESIGNING A DISTORTION GAUZE FOR TESTING A BOUNDARY LAYER INGESTING FAN

Tomasz Kwiatkowski *, **Adam Sieradzki**, **Borys Łukasik**
Łukasiewicz Research Network – Institute of Aviation, al. Krakowska 110/114, 02-256 Warsaw, Poland

Abstract

As global trends aim to reduce emissions of pollutants, boundary layer ingesting (BLI) propulsions are attracting more and more attention. As such, N+2 generation aircraft with propulsion placed in the aft of the aircraft are gaining in popularity. The boundary layer is formed on the fuselage before entering the engine located in the aft of the aircraft. Due to significant difficulties in performing experimental tests of BLI propulsors with full-size aircraft, distortion gauzes are one of the methods to provide the desired air velocity profile at the inlet. This paper describes a novel method of designing such gauzes, a topic which is not well covered in the existing literature. In the first stage of the presented method, single orifices of different sizes were calculated using CFD tools. The relationship between their size and the gauze resistance coefficient was identified, making it possible to model the distortion gauze using porous media. An iterative approach was used to design a gauze that meets the requirements. This is, to our knowledge, the first distortion gauze design description where a porous media model has been used. Experimental tests demonstrated that the produced distortion gauze yields a velocity profile comparable to the desired one. This indicates the great potential of using the presented approach in further research on boundary layer ingesting propulsions. It offers an opportunity to reduce substantially both the costs of experimental research and the time required to design a distortion-tolerant fan.

Keywords: boundary layer ingestion; distortion gauze; porous media; distorted velocity profile
Type of the work: research article

Nomenclature

A	area of a hexagon	p_0	ambient pressure
d_h	calculated hydraulic diameter of orifice	Δp	pressure drop
D	diameter of the channel	Re	Reynolds number
f_0	open area of one orifice	S_i	source term
$\overline{f}$	porosity	v	kinematic viscosity of the fluid
h	height of open orifice in a hexagon	V	velocity magnitude
H	base height of orifice in gauze	w_o	velocity in the orifice
$\overline{l}$	gauze thickness nondimensionalised by the height of the hexagonal orifice	α	permeability
		ρ	density
l	total gauze thickness	Π_0	perimeter of the orifice
K	gauze resistance coefficient		

* Corresponding Author: tomasz.kwiatkowski@ilot.lukasiewicz.gov.pl
ARTICLE HISTORY **Received** 2021-10-08 **Revised** 2022-01-18 **Accepted** 2022-02-11

1. INTRODUCTION

In recent years, growing popularity of boundary layer ingesting engines has been observed [1]. Since these engines are mounted in the aft of the aircraft, it is possible to compensate for momentum loss in the aircraft wake by means of the momentum coming from the exhaust outlet [2]. Thus, an up to approx. 5% fuel burn reduction could be achieved with five engines embedded into the upper aft surface of a hybrid wing body aircraft over a 7500nm mission [3]. The boundary layer ahead of the engine intake is developed on the aircraft's fuselage [4]. During wind tunnel experiments, however, there is often insufficient space for the use of a fuselage to develop the boundary layer [5]. For example, the following mechanisms were used in NASA's 8' x 6' supersonic wind tunnel in order to produce the desired velocity profile: floor roughness, test section porosity and a bleed box connected with a bleed system to adjust the boundary layer thickness [6]. All additional mechanisms installed to develop the boundary layer increase the cost and size of the test rig.

In order to overcome these difficulties, a velocity profile can be formed with the use of a distortion gauze. This is accomplished by using a distortion gauze with varying orifice size. One of the first works on improving the velocity field in flow was Prandtl [7], which indicated the possibility of reducing turbulence behind a wire gauze using a honeycomb structure. Attempts were made to understand the effect of wire gauze on the flow field [8], [9], [10]. The relationship between the Reynolds number and the square mesh wire gauze resistance coefficient was shown, but the empirical coefficients used in the relationships were not explained [11]. Further work showed that it is possible to obtain nearly uniform shear flow by inserting a variably spaced grid of parallel rods [12]. In further work [13], attempts were made to derive theoretical equations that allow the assumed velocity profile to be attained, for example by introducing arbitrarily-shaped parabolic gauzes. It was also realized that in practical applications, the dependence of the gauze resistance coefficient on the Reynolds number may be neglected. Problems of this type can be solved using relatively simple numerical techniques, but they apply to wire gauzes of arbitrary resistance variation. However, the experimental results were of poor quality [14]. Previous theories were continually modified to achieve better agreement with the experiment, but still the way to achieve the desired velocity profile was to use gauze in which the screen angle varies across the duct [15].

1.1. Objective

The objective of the present study was to find a method able to save design time and costs associated with experimental research. Previous distortion gauze designs used data from measuring the resulting pressure loss from several test pieces of gauze with known solidities [17]. The disadvantage of this approach is the need to incur additional expenses for making gauzes with different porosities and measuring them experimentally, thus unnecessarily prolonging the design time. A study by Idelchik [16] presents an experimental formula showing the relationship between the porosity of the orifice, its thickness and the resistance coefficient. Unfortunately, as the article shows, this relationship is only valid for meshes with constant porosity and cannot be used in practical application (in gauzes with variable porosity) due to the fact that perpendicular velocity components were not taken into account.

Seeking to avoid these discrepancies, the present article presents a novel method of designing a distortion gauze using a porous media model that provides better agreement with the experiment. We hypothesize that it is possible to design a distortion gauze using only computational fluid dynamics (CFD) methods – an original methodology that has not been described in the literature, which allows for significant savings in design-related time and costs.

2. METHODOLOGY

2.1. Gauze design assumptions

The initial step of the design process requires the following assumptions. The diameter of the channel was set to D=0.58m, equal to the diameter of the inlet duct in our test rig. The density was assumed as 1.225 kg/m^3. The assumed mass flow rate corresponds to the design operating conditions of the fan. Uniform flow was assumed at the inlet to the duct, but due to the presence of the distortion gauze, velocity redistribution takes place upstream of the gauze. The desired velocity profile is obtained in the section located upstream of the test fan. A similar simplification of the problem was adopted by Whittle Laboratory in their BLI test program [17]. The distortion gauze is assembled with the flow straightener. The purpose of the flow straightener is to damp transient transverse velocity oscillations and suppress turbulence intensity downstream from the gauze. Assumed distorted velocity profile (Figure 1) was obtained by reading the contour plot from study [17] using MATLAB algorithms, converting RGB colour map into velocity magnitude values. The above-mentioned velocity profile was used in the SAX-40 (Silent Aircraft eXperimental airplane) CFD calculations. Figure 1 presents the velocity contour after the profile is scanned and rendered non-dimensional using a maximum value. The X is the streamwise direction, while Y and Z are orthogonal to X.

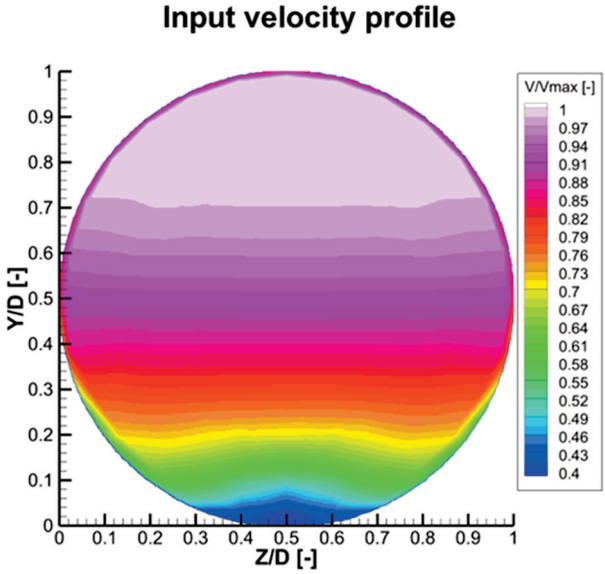

Figure 1. Reference velocity profile that should be achieved by the designed distortion gauze by using CFD methods. [17]

2.2. Gauze design procedure

A specific algorithm was developed and used to design the gauze. To obtain a desired velocity profile some additional assumptions were made. A honeycomb-shaped distortion gauze was chosen. The convention and symbols describing the orifice size are presented in Figure 2.

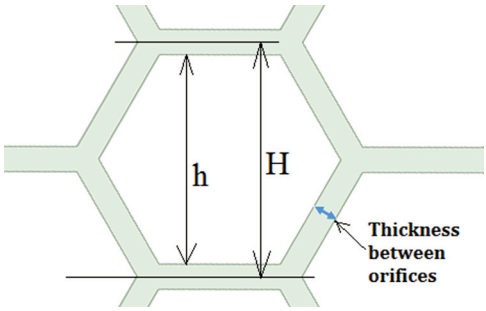

Figure 2. A fragment of the distortion gauze in which hexagonal orifices were used. The orifice height h, the base orifice size H and the thickness between the orifices are taken into account.

As the orifice base height H decreases, the pressure drop increases due to more obstacles in the flow, but on the other hand, the velocity profile might be smoother. Initially, the number of orifices along the Y axis of the channel was set to 67 and along the Z axis to 58, as a trade-off between acceptable pressure drop and the quality of the desired velocity profile. The number of grid cells differs in perpendicular directions because the honeycomb shaped orifices partially overlap. The minimum distance between two consecutive orifices (thickness of the orifice wall) was initially set to $H/10$, so the maximum assumed height of the open orifice is $h=9H/10$. Lower thickness could result in potential gauze damage, due to stress caused by moving air. On the other hand, higher minimum thickness could lead to higher losses generated by the gauze. The area of the internal and the external hexagon can be expressed as follows:

$$A_{internal} = \frac{h^2\sqrt{3}}{2}, \tag{1}$$

$$A_{external} = \frac{H^2\sqrt{3}}{2}. \tag{2}$$

Porosity $\overline{f}$ is the ratio of the area of internal to external hexagon. Thus, the porosity of the single orifice is defined by the following equation:

$$\overline{f} = \frac{A_{internal}}{A_{external}} = \frac{\frac{h^2\sqrt{3}}{2}}{\frac{H^2\sqrt{3}}{2}} = \frac{h^2}{H^2}. \tag{3}$$

The boundary layer develops naturally in the vicinity of the walls on the perimeter of the channel, as presented in Figure 1. To simplify the design process, the boundary layer was completely removed from the initial velocity profile. According to [16], gauze resistance coefficient is a function of porosity and total thickness l of the gauze. Relatively low gauze resistance is obtained for the non-dimensional parameter l/d_h in the range between 0.2-3. Outside this range, the gauze resistance increases. The diameter d_h is the calculated as the hydraulic diameter of the orifice located in the middle of the gauze. Total thickness of the distortion gauze was set to 2mm in order to provide a compromise between its high stiffness and low resistance.

2.3. Resistance of the orifice

For the assumed velocity of about 28m/s and orifice diameter of 6-9mm, the expected range of Reynolds numbers is between Re=1e4-1.7E4. It was decided to express gauze resistance coefficient as a function of porosity using CFD calculations since available experimental data is valid only for $Re>10^5$. For the conditions specified in [16], where $\overline{l}$ is the total gauze thickness l nondimensionalised by calculated hydraulic diameter of the orifice d_h (expressed as (5)) and Reynolds number greater than 100000:

$$\overline{l} = \frac{l}{d_h} > 0.015 \quad \text{and} \quad \mathrm{Re} = \frac{w_o \cdot d_h}{v} \geq 10^5, \tag{4}$$

$$d_h = 4 \cdot \frac{f_0}{\Pi_0}. \tag{5}$$

Coefficient τ can be calculated using equation (6), where $\varphi\left(\overline{l}\right)$ is the coefficient defined by equation (7):

$$\tau = \left(2.4 - \overline{l}\right)^{\varphi\left(\overline{l}\right)}, \tag{6}$$

$$\varphi\left(\overline{l}\right) = \frac{0.25 + 0.535\overline{l}}{0.05 + \overline{l}^{\,7}}. \tag{7}$$

Finally, the gauze resistance coefficient as a function of porosity [16] can be calculated using the following empirical formula [16]:

$$K = \frac{0.5\left(1-\overline{f}\right)^{0.75} + \tau\left(1-\overline{f}\right)^{1.375} + \left(1-\overline{f}\right)^2 + \lambda\dfrac{l}{d_h}}{\overline{f}^{\,2}}. \tag{8}$$

It was reported that flow through gauzes represents weak dependence on Reynolds number [13], but the mentioned [16] limitation of Reynolds number $Re>10^5$ evokes additional uncertainties, so it was decided to perform CFD calculations in conditions that match those from the planned experiment. Figure 3 shows a fragment of the geometry of the designed distortion gauze with constant orifice size. Performing numerical calculations for the entire gauze would be very costly in terms of computation and time. The distortion grid contains almost 4,000 holes. Based on x+, y+ and z+ requirements, if at least 30 mesh nodes were defined for each orifice in each direction, each orifice would have approximately 27,000 finite volume cells. After multiplying the number of mesh cells per orifice with the number of orifices (approximately 4,000), the computational domain would contain at least 108 million cells only inside the gauze orifices. In addition, it is necessary to generate additional cells in the streamwise direction to take into account the velocity redistribution before the distortion gauze. As a result, the computational mesh would be very large.

One of the objectives of this paper is to show that it is possible to design a distortion gauze without the need to generate such huge computational meshes. It is possible and necessary to include a single orifice, as this is sufficient to find the relationship of porosity to resistance. This relationship will be used to adjust the velocity profile for the porous model. At first glance, the limitation of this approach might be that the perpendicular velocity components are not taken into account, but the interaction between

the orifices is included in the source term model. This limitation may affect the difference of about 10% between the assumed and obtained velocity profile, as will be presented in the part of the article where the results are compared with the experiment. This limitation is reduced when a porous media model is used.

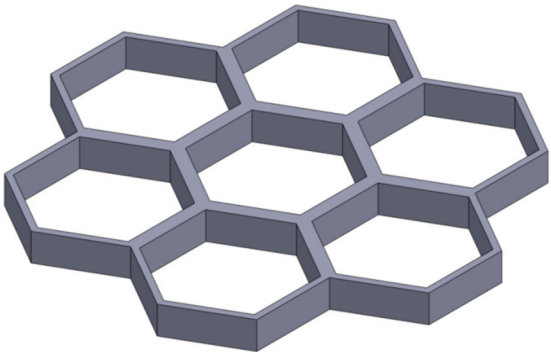

Figure 3. Sample geometry of a distortion gauze of a certain thickness, in which hexagonal orifices were used to present the idea of the distortion gauze shape.

3. NUMERICAL CALCULATIONS

3.1. Computational approach

To reduce the aforementioned difficulties, it was decided to perform numerical calculations of a series of single orifices with different porosities. Thanks to that the dependence of resistance for a given porosity of the orifice diameter will be known. In the next stage, this allows the relationship between porosity and the resistance of a given porosity to be identified. A CAD model representing the air volume crossing a single orifice (Figure 4(a)) was created. Figure 4 (a) shows a schematic of the model containing a local reduction in cross-section simulating the presence of a distortion gauze in the flow. The inlet is marked in blue, the symmetry is marked in yellow, and the "wall" boundary conditions are marked in gray. Because the hexagonal section has a point of symmetry, only one sixth of the section can be modelled. To further reduce both time and cost of the CFD analysis, it was also decided to use $1/6^{th}$ of a modelled volume of the hexagonal orifice along with periodic boundary conditions, shown schematically in Figure 4 (b). This allows the number of mesh cells to be reduced while maintaining high quality mesh. Computational domain has a length of 400mm and contains a screen with a thickness of 2mm. Calculations were performed using the k–ω SST model. Velocities of 10, 20, 28 and 40 m/s were specified at the inlet with the use of velocity-inlet boundary condition. The velocities are suitable for a low-pressure fan.

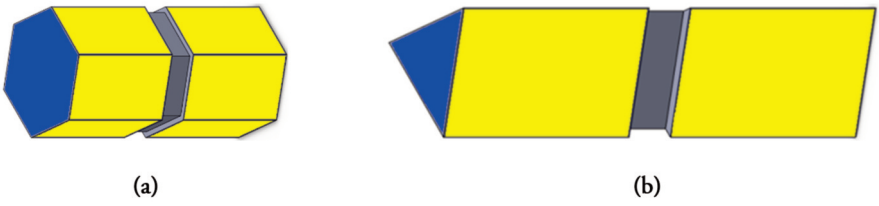

Figure 4. Single orifice computational domain diagram. The inlet is marked in blue, the boundary condition of symmetry is marked in yellow, and the boundary condition wall is marked in gray. There is an outlet on the invisible side. Figure (a) shows the full geometry of the orifice, and Figure (b) shows a $1/6^{th}$ fragment of the orifice. In addition, in Figure (b), the periodicity condition is invisible.

3.1.1. Grid dependence study for a single orifice

The ANSYS Fluent commercial software was used for the calculations. The velocity-inlet boundary condition with the set velocity values was used at the inlet. At the outlet of the domain, the pressure outlet boundary condition without forced flow was used. The k–ω SST turbulence model was used, as was the case for further calculations of the entire distortion gauze. The grid dependence study was performed to ensure high quality of mesh and a trade-off between grid size and calculation accuracy. In order to select the optimum grid size for the single orifice of high porosity, grid dependence studies were carried out. Four grids with 37,776, with 89,552, with 180,178 and with 380,522 nodes were investigated. The results of grid dependence studies are presented in Table 1, which shows the number of mesh nodes, the Y+ parameter and the pressure drop. Pressure drop Δp was calculated as a difference between static pressure measured 150 mm upstream and downstream from the orifice. The pressure drop was chosen for the mesh density study because it determines the resistance of the orifice and, consequently, the relationship between porosity and resistance. As the number of grid cells increases, the pressure drop does not change significantly. It was observed that there is a low difference (around 1 pascal) between mesh 2 and mesh 4 (the finest), and therefore mesh 2 was used for further calculations of a single orifice.

Table 1. Comparison of the parameters of the meshes used for the grid dependence study.

Mesh	Number of nodes	Y+ parameter	Pressure drop [Pa]
Mesh 1	37,776	2.3	152.35
Mesh 2	89,552	~1	155.44
Mesh 3	180,178	<1	155.19
Mesh 4	380,522	<1	156.32

The computational Mesh 2 containing 89,552 nodes is depicted in Figure 5, with every second node of the grid shown. It was decided to use an ICEM mesh generator. The computational mesh contains 4 blockings, each of which contains a structural grid. Near the walls, the mesh was refined, keeping the Y+ parameter less than 1. One of two periodic surfaces is visible and marked in blue. The area on which the symmetry boundary condition has been defined is marked in yellow. Moreover, "wall" surfaces are marked in gray. Just before the orifice (viewed from the direction of flow), a white control cross-section is shown showing the computational mesh.

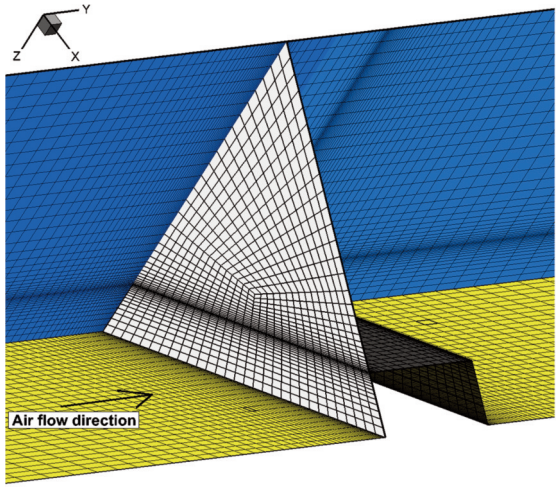

Figure 5. View of the computational grid on the boundaries of the computational domain of 1/6th of the orifice, also shown in white, the cross-section just before the orifice. The periodic boundary condition is marked in blue and the symmetry boundary condition is marked in yellow. Wall is marked in gray. Every second mesh node is shown.

Orifice resistance was calculated using CFD methods. Taking into account different porosities varying from 0.3 to 0.9 with a constant interval of 0.1, orifice resistance was calculated using equation (9). Static pressure distribution along the X axis of the domain for porosities of 0.5 and 0.7 and velocity magnitude 28m/s is presented in Figure 6.

$$K = \frac{2\Delta p}{\rho V^2}. \tag{9}$$

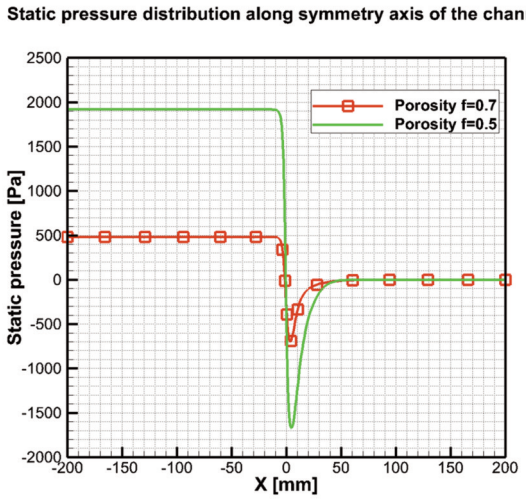

Figure 6. Distribution of static pressure along the axis of the orifice for the velocity magnitude 28m/s and porosity $\overline{f}$ = 0.5 and $\overline{f}$ = 0.7. For smaller porosity, a larger pressure drop is visible. The pressure drop was measured in cross-sections 150mm before and after the orifice.

As presented in Figure 6, static pressure remains constant when measured 150 mm upstream and downstream from the orifice. This confirms that the pressure drop can be calculated using the equation shown in (10). Furthermore, the pressure drop was used for calculations of gauze resistance coefficient. This allowed the relationship to be identified between each porosity and the gauze resistance coefficient.

3.2. Function of porosity and resistance

The porosity as a function of orifice resistance was approximated and presented in Figure 7. Red squares present the data obtained from a series of CFD calculations. The red line presents the approximated correlation of porosity as function of gauze resistance coefficient for single value of velocity 28m/s. This correlation was used in further calculations. The blue line shows the experiment based correlation [16]. The difference between CFD results and experimental formula was less than 4%. It should be emphasized that the experimental formula was obtained for higher Re, which shows that flow through gauzes represents weak dependence. Unfortunately, this equation is not suitable for designing the distortion gauze, because it does not take into account the perpendicular velocity components that occur at flow redistribution before the gauze. In addition, this relationship does not take into account differences of streamwise velocities in orifices with different porosities, because this relationship is valid only for single velocity value of 28m/s, which might slightly affect the resistance coefficient. To avoid these simplifications, a porous media should be defined for the range of porosities and velocities. The green line shows the relationship

between the gauze resistance coefficient and porosity predicted by the porous structure described later in the article, assuming a constant porosity throughout the modelled gauze. This difference may partly explain the discrepancies in the results described below.

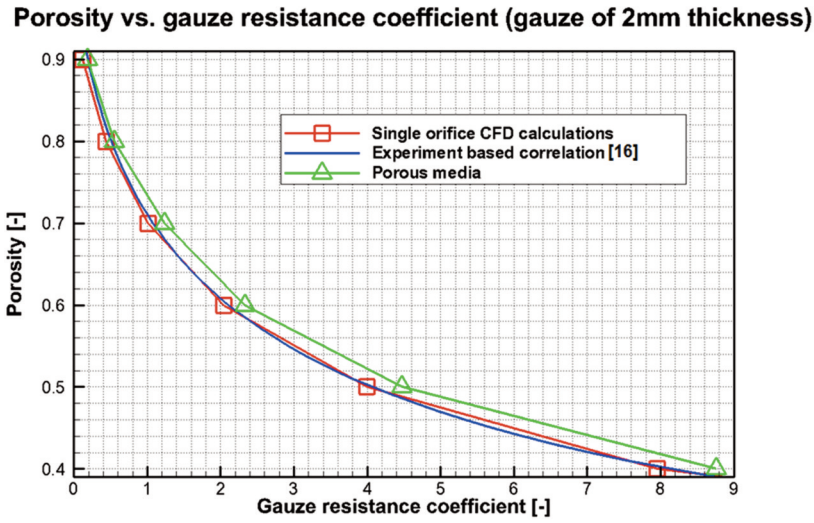

Figure 7. Comparison of the dependence of porosity as a function of the orifice resistance coefficient for single orifice cases calculated in CFD (marked with a red line with squares), experimental dependence (marked with a blue line) [16] and predicted by porous media (from the next step, marked in green).

3.3. Distribution of resistance and porosity

Pressure drop Δp of the entire gauze can be approximated by taking into account a minimum gauze resistance $K_{\min}$ (which corresponds to the maximum expected porosity 0.81 and equals 0.406) and maximum velocity in the channel for given velocity distribution for which the desired mass flow rate is obtained. To calculate the pressure drop Δp of the entire gauze, the following equation should be used:

$$\Delta p = K_{\min} \frac{\rho V_{\max}^2}{2}. \tag{10}$$

The pressure drop is necessary to calculate the distribution of the resistance along the gauze. The gauze resistance coefficient distribution must be computed as a function of the velocity at a selected location of the gauze:

$$K(r,\varphi) = \frac{2\Delta p}{\rho \cdot \left(v(r,\varphi)\right)^2}. \tag{11}$$

Furthermore, the gauze resistance distribution $K(r, \varphi)$ must be converted to the porosity distribution $\overline{f}\,(r, \varphi)$. This can be done by using the formula of porosity as function of resistance on the basis of CFD simulations of individual orifices, presented in the previous paragraph. Once the porosity distribution $\overline{f}\,(r, \varphi)$ is obtained, the momentum equations for porous media $S_i(r, \varphi)$ can be defined.

3.4. Numerical analysis of a porous media

As mentioned above, due to the high computational cost, it is difficult to perform numerical calculations of the airflow through the distortion gauze. To reduce computational costs, a porous media model was used to simulate the distortion gauze. By performing numerical calculations of single orifices for the range of velocity and porosity, it is possible to define the source term. Three-dimensional porous media takes into account perpendicular velocity components and is necessary to obtain the correct velocity distribution. In order to define porous media, orifice resistance coefficient for varying porosities must be used. Porous media are modelled by the addition of a momentum source term to the standard fluid flow equations which is composed of the following parts:

- viscous loss term:

$$\frac{\upsilon}{\alpha} V_i, \tag{12}$$

- inertial loss term (C_2 is the inertial resistance factor):

$$C_2 \frac{1}{2} \rho |V| V_i. \tag{13}$$

Considering the case of simple homogenous porous media, the source term for the *i*-th momentum equation can be expressed as:

$$S_i = -\left(\frac{\upsilon}{\alpha} V_i + C_2 \frac{1}{2} \rho |V| V_i \right). \tag{14}$$

A simplified version of the momentum equation, relating the pressure drop to the source term, can be expressed as in equations (15) and (16):

$$\nabla p = S_i, \tag{15}$$

$$\Delta p = -S_i l. \tag{16}$$

Total pressure drop can furthermore be expressed as follows, where *a* and *b* are the second order polynomial coefficients. Approximation polynomials (17) for the analysed porosities are presented in Figure 8.

$$\Delta p = aV^2 + bV. \tag{17}$$

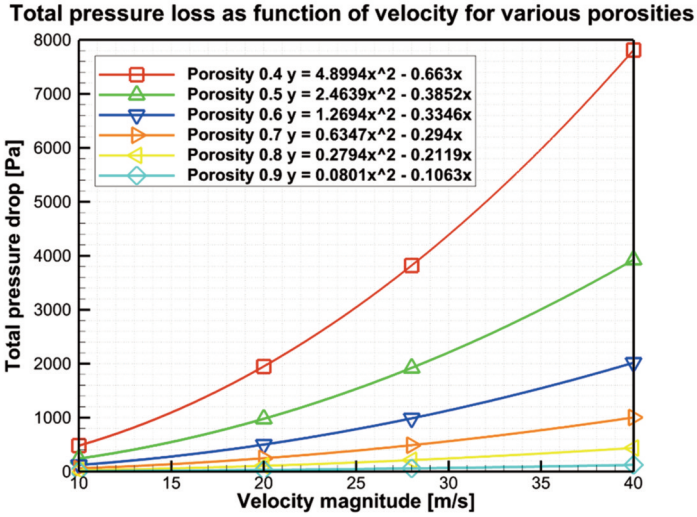

Figure 8. Total pressure drop as a function of velocity magnitude for the analyzed porosity values from 0.4 to 0.9. For each porosity, a second order polynomial equation is presented that blends pressure drop with velocity.

Thus the inertial resistance factor and permeability for each porosity may be calculated using the following equations (18) and (19).

$$C_2 = \frac{2a}{\rho l}\left[\frac{1}{\mathrm{m}}\right], \tag{18}$$

$$\frac{1}{\alpha} = \frac{b}{vl}\left[\frac{1}{\mathrm{m}^2}\right]. \tag{19}$$

In the last step of defining the porous structure, the equation binding inertial resistance factor and permeability to porosity should be found. It was noted that a good approximation can be obtained by using a polynomial of a degree equal to the number of porosities used. Porosity is then used as the input parameter to define the parameters of the porous structure. The parameters of porous structure are being projected into the computational nodes of the mesh.

In order to reduce turbulence behind the gauze, a flow straightener was used in the experiment. Due to its high porosity, this straightener causes low resistance. It is worth mentioning that ANSYS Fluent solves the standard conservation equations for turbulence quantities in the porous medium, so the turbulence field is only approximated. It is assumed that the porous media does not affect the intensity of turbulence or dissipation rates. This may be a source of discrepancy between CFD results and the experiment and might be discussed in further work.

3.4.1. Grid dependence study for a channel

A mesh density study was also carried out for a three-dimensional channel. In order to save computational effort, half the channel was simulated with the symmetry boundary condition. Three computational grids with different densities and different number of cells along the channel diameter were created, according to the data presented in Table 2. In grids of various densities, the number of grid cells inside the porous structure, which simulated the distortion grid, also changed. The impact of mesh density on the total pressure distribution is shown in Figure 9. The pressure distribution was chosen for the mesh density study because the velocity distribution depends on it. The exact velocity distribution is the output parameter we want to achieve. In the coarse grid, there is a slight difference in total pressure distribution between Y/D = 0.5 and Y/D = 0.8. Since the medium mesh corresponds well to the predictions of the fine mesh, it was decided to use the medium mesh in further calculations. Calculations carried out converged well and took about an hour on the single node of the high performance computing cluster. This allows for a significant time saving compared to the approach with simulating a real-shaped distortion gauze taking into account the exact shape of the orifices.

Table 2. Comparison of the parameters of the meshes used for the grid dependence study.

Mesh type	Total number of cells	Number of cells in the porous zone	Number of cells along diameter
Coarse mesh	85,692	5,404	62
Medium mesh	396,936	25,032	134
Fine mesh	2,495,362	57,438	162

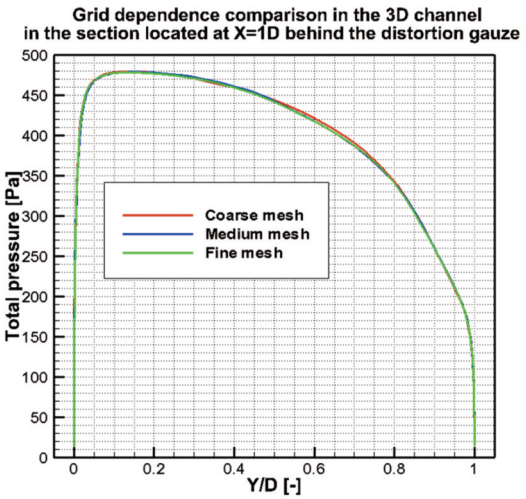

Figure 9. Comparison of the total pressure distribution for different densities of the grids along the diameter of the three-dimensional channel in the cross-section located 1 diameter of the channel behind the distortion grid.

3.5. Adjusting gauze parameters

Porous media was used to model a distortion gauze inside half of the 3D round channel. To maintain accuracy and comparability with single orifice calculations, all the 3D test cases were calculated using the k–ω SST turbulence model, as was previously used. The mass-flow-rate boundary condition was

applied at the inlet. Adjustment of the gauze parameters was performed iteratively. At each iteration the velocity profile predicted with the use of CFD tools was compared with the desired velocity profile. If predicted velocity profile differed from the desired one, input velocity profile (understood as used for porosity calculations) was corrected by the difference between the velocity values. After correcting the input velocity profile, the resistances and porosity were recalculated according to the procedure described earlier. From the porosity distribution the porous media was defined, which after CFD calculations of 3D channel gave the velocity distribution. Seven iterations were necessary to obtain good agreement between analysed velocity profiles. Comparison between velocity profiles obtained during the 1st and 7th iteration is presented in Figure 10. In the first stage, the desired velocity profile presented in was used as the input velocity profile. It turned out that there is a large discrepancy between the assumed and predicted velocity distribution. The difference in distorted region might be caused by the fact that formula describing the gauze resistance coefficient as a function of porosity is defined only for a single velocity, equal to 28m/s. Another source of discrepancy is the vertical velocity components caused by the change in orifice size along the distortion gauze, which were neglected in this formula. Vertical velocity components could be omitted in single orifice calculations, because the goal was to find the relationship between porosity and orifice resistance for the Reynolds numbers used in our gauze design. The porous structure takes into account vertical velocity components during calculations, which allows for more accurate prediction of the flow field, which will be demonstrated in comparison with the experiment later in the work. The velocity predicted by source term calculated for the range of porosities and velocities was used as reference during the next iterations. In subsequent iterations of the distortion gauze design, the previously determined dependence of porosity as a function of the orifice resistance coefficient was used. In turn, the orifice resistance coefficient is a function of velocity, as shown in equation (11). Porosity is the input value for a porous media. The velocity distribution is the output value for a given porosity distribution $\overline{f}(r, \varphi)$. The purpose of the iterative process is to adjust the porosity in such a way as to achieve the assumed velocity profile.

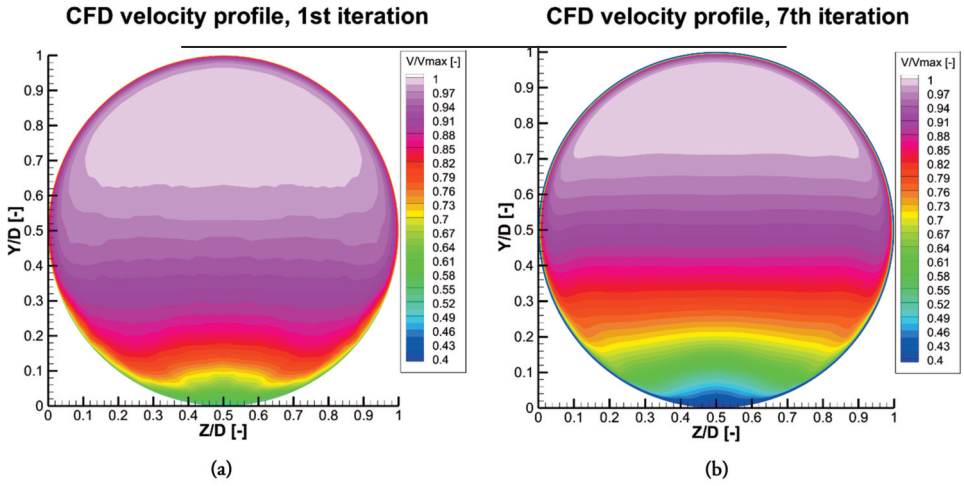

Figure 10. Comparison of velocity profiles obtained during iterative process: (a) velocity profile predicted by the porous media based on the reference velocity profile shown in Figure 1. In the right Figure (b) is shown the velocity profile predicted by the porous media after adjustments of input velocity profile.

3.6. Gauze generation

Once the desired velocity profile is obtained, orifice height distribution must be calculated as a function of porosity using equation (20) derived from equation (3):

$$h(r,\varphi) = \sqrt{\frac{H^2}{\bar{f}(r,\varphi)}}. \tag{20}$$

Base height H was assumed constant and equal to 10mm. CAD model of the distortion gauze is presented in Figure 11 (a), and Figure 11 (b) shows the manufactured gauze after laser cutting. This gauze was used in the experiment described in the next section.

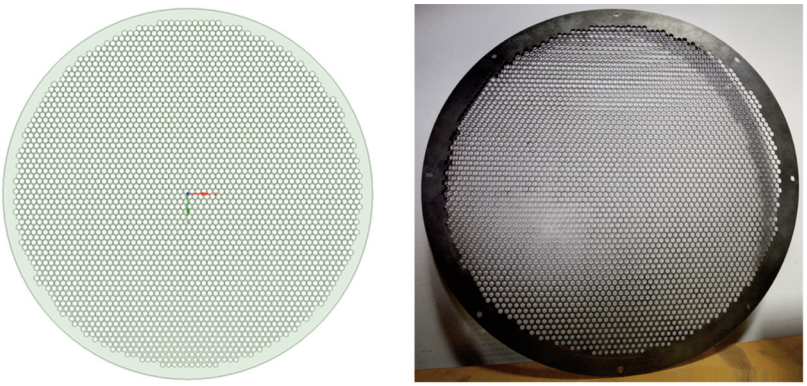

(a) (b)

Figure 11. CAD model (a) of the distortion gauze with final porosity and the corresponding actual distortion gauze (b) that has been laser cut. Mounting holes are also visible.

4. EXPERIMENT SETUP AND RESULTS

The scheme of the test stand is shown in Figure 12, where the air is being sucked in through the bell-mouth inlet. The distortion gauze and flow straightener are located approximately 0.7m upstream of the rotor. The velocity profile measurement section is placed about 0.2m downstream (section 2). The required mass flow rate value is obtained by adjusting the position of a throttle cone in the aft part of the test stand. The rotor and stator were designed using T-Blade software and further optimized using genetic algorithms to guarantee proper performance in axisymmetric flow [18], [19]. Another subsequent study will be focused on redesigning the fan for the purpose of non-axisymmetric flow.

Measurements of the distorted velocity profile were performed with the use of five-hole pressure probes mounted on a dedicated traverse mechanism. This traverse system allows the probe position to be changed radially and circumferentially. With the use of predefined map of measurement points, the discussed system allows fully automatic and precise cross-sectional measurements to be performed. All the searched values were averaged over 3-second measurements. The probes measure the value of total and static pressure and the direction of the velocity vector of the flow. Air density was calculated based on air temperature and humidity measurements. Both the difference between total and static pressure and the density were used during post processing to calculate the velocity magnitude value at every point of the map. The section area was mapped using 5120 points with 40 different radial positions of the probe.

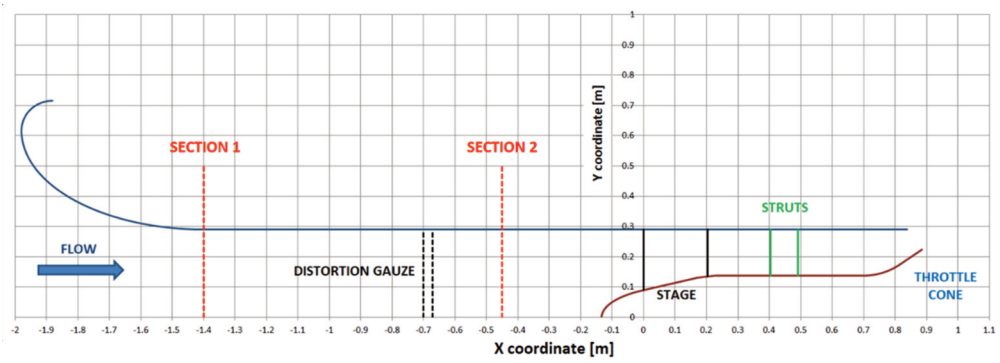

Figure 12. Scheme of test rig. A bellmouth inlet has been defined at the inlet. The distortion gauze was placed 0.7m in front of the leading edge of the rotor. Sections 1 and 2 are measuring sections in which flow parameters were measured. At the outlet, mass flow rate is regulated by changing the position of the throttle cone.

The measured velocity profile is nondimensionalized and presented in Figure 13. To expose the differences between the assumed and the obtained velocity profile, velocity values were calculated at the vertical centerline defined by Z/D=0 and compared in Figure 14. In the region of distorted flow (Y/D=0.9 to Y/D=1), the differences between the measured and predicted velocity does not exceed 5%. These small differences may be caused by the fact that transient structures are filtered during RANS calculations. It is also clear that the velocity distribution obtained in the experiment is closer to the distribution obtained in the last iteration of the numerical calculations of porous media. This proves that the experimental formula [16] as well as formula based on single orifice CFD calculations formulas shown in Figure 7 cannot be used to design a gauze with variable porosity. Considering the use of a low-order (low-cost) porous model, the obtained results show very good agreement with the experiment. Compared to the methods of designing gauzes using a set of real gauzes with different porosities, the proposed method using CFD shows the great advantage of the proposed approach. The proposed approach allows for significant savings in design time and costs.

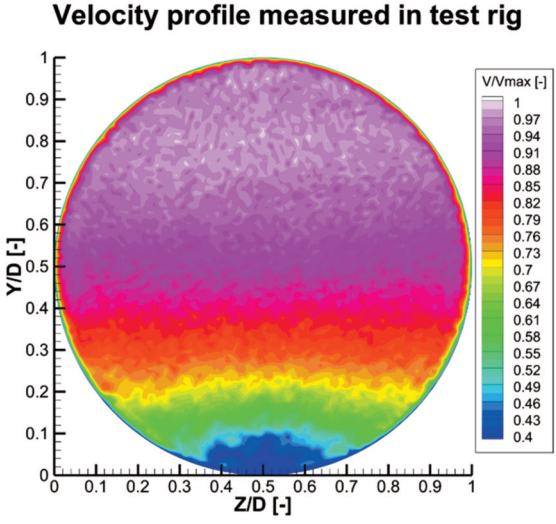

Figure 13. Velocity profile measured in section 2 located 0.25m behind the distortion gauze.

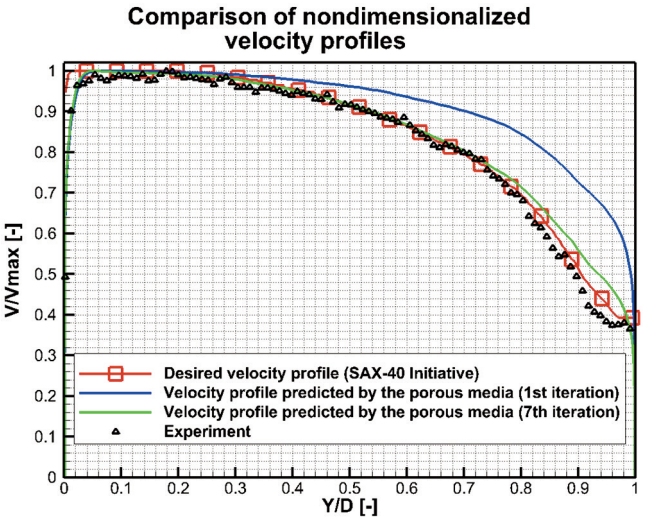

Figure 14. Comparison of velocity profiles in the middle line of velocity contour (Z/D=0). The red color line with squares indicates the velocity profile proposed by SAX-40 Initiative. The blue line shows the velocity profile obtained in the first iteration that required adjustments. The acceptable speed profile obtained in the last iteration is shown in green. Moreover, the black triangles show the velocity profile measured in the experiment.

5. CONCLUSIONS

This paper presents a methodology for designing a distortion gauze used to produce a specific velocity profile in the inlet duct of an axial fan. A distortion gauze is a special case of a porous medium with the flow direction parallel to the fan axis. In this type of application, straighteners are used and inflow angles are assumed to be close to zero. In a full flight transient, the angles of attack in the velocity profile would be variable; this could be a topic for future work.

Research shows that the functionality of structures of this type can be successfully modelled with the use of commonly known models of porous media. However, this requires the determination of equivalent resistance of the porous structure. The tools developed and methodology adopted herein allow for very fast and effective simulation of the distorted velocity profile creation in the channel, and can be successfully used in the design process of a distortion gauze. It is of crucial importance in processes of testing unevenly loaded fan and makes it possible to more accurately represent its operating conditions on the test rig. On the basis of the author's experimental data it was stated that the model of porous medium allows to determine the velocity profile with an absolute error not exceeding 5%. In future work, it is also proposed to focus on ways to improve the porous structure model leading to reducing differences from the experiment.

Funding: This research was funded by a subsidy granted by the Ministry of Education and Higher Education of the Republic of Poland.

Acknowledgments: The research reported herein was carried out as part of the BLI-Fan research program which was one of the outcomes of the Polish-American partnership and collaboration between the Łukasiewicz Research Network – Institute of Aviation and the Ohio State University. The authors would like to acknowledge Professor Meyer J. Benzakein affiliated with the Ohio State University for being the co-founder of this cooperation, as well as for his invaluable support and technical contribution to this research. The authors would like also to express their gratitude to the members of the BLI-Fan task group, for their contribution and vast commitment into this research.

REFERENCES

[1] Hardin, L. W., Tillman, G., Sharma, O. P., Berton, J., Arend, D.J. "Aircraft System Study of Boundary Layer Ingesting Propulsion." *48th AIAA/ASME/SAE/ASEE Joint Propulsion Conference & Exhibit,* 30 July – 01 August 2012, Atlanta, Georgia.

[2] Uranga, A., Drela, M., Hall, D. K., Greitzer, E. M. "Analysis of the Aerodynamic Benefit from Boundary Layer Ingestion for Transport Aircraft." *AIAA Journal* 56:11 (2018): pp. 4271–4281

[3] Arend, D.J., Tillman, G., O'Brien, W. F. "Generation After Next Propulsor Research: Robust Design for Embedded Engine Systems." *48th AIAA/ASME/SAE/ASEE Joint Propulsion Conference & Exhibit*, 30 July – 01 August 2012, Atlanta, Georgia.

[4] Madani, V., Hynes, T. P. "Boundary Layer Ingesting Intakes: Design and Optimization." *Proceedings of XIX International Symposium on Air Breathing Engines* (2009). ISABE Paper No. 2009–1346.

[5] Florea, R. V., Voytovych, D., Tillman, G., Stucky, M., Shabbir, A., Sharma, O., Arend, D.J. "Aerodynamic analysis of a boundary-layer-ingesting distortion-tolerant fan." *Proceedings of ASME Turbo Expo 2013: Turbine Technical Conference and Exposition*, June 3–7, 2013, San Antonio, Texas, USA.

[6] Hirt, S. M., Arend D. J., Wolter J. D., Johnson, A.M. "Development of a Flow Field for Testing a Boundary-Layer-Ingesting Propulsor." *53rd AIAA/SAE/ASEE Joint Propulsion Conference*. July 2017.

[7] Prandtl, L. "The Attainment of a Steady Air Stream in Wind Tunnels." *Handbuch der Experimentalphysik*. Vol. 4, Part 2, pp. 65–106. *NACA Technical Memorandum 726*, October 1933.

[8] Collar, A. R. *The effect of a gauze on the velocity distribution in a uniform duct*. Aeronautical Research Committee in London (1939).

[9] Simmons, L. F. G., Cowdrey, C. F., Sir Taylor, G. I. "Measurements of the aerodynamic forces acting on porous screens." *Reports and memoranda (Aeronautical Research Council (Great Britain)), no. 2276* (1945).

[10] Taylor, G. I., Batchelor, G. K. "The Effect of Wire Gauze On Small Disturbances in a Uniform Stream." *Quart. Journ. Mech. and Applied Math*. Vol. II, Pt. 1 (1949).

[11] Davis, G. *Non-uniform flow through wire screens*. Ph.D. Dissertation, University of Cambridge, 1957.

[12] Owen, P. R., Zienkiewicz, H. K. "The production of uniform shear flow in a wind tunnel." *Journal of Fluid Mechanics*, Volume 2, Issue 6, August 1957, pp. 521–531.

[13] Elder, J. W. "Steady flow through non-uniform gauzes of arbitrary shape." *Journal of Fluid Mechanics*, vol. 5 (1959): pp. 355–368. DOI: 10.1017/S0022112059000258.

[14] Turner, J. T. "A computational method for the flow through non-uniform gauzes: the general two-dimensional case." *J. Fluid Mech*. Vol. 36, part 2 (1969): pp. 367–383.

[15] Livesey, J. L., Laws, E. M. "Flow through non-uniform gauze screens." *J. Fluid Mech*. Vl. 59, part 4 (1973): pp. 737–743.

[16] Idelchik, I. E. *Handbook of hydraulic resistance: Coefficients of Local Resistance and of Friction.* Begell House (1996), ISBN: 1567000746.

[17] Gunn, E. J., Hall, C. A. "Aerodynamics of Boundary Layer Ingesting Fans." *Proceedings of the ASME Turbo Expo 2014: Turbine Technical Conference and Exposition*. Volume 1A: Aircraft Engine – Fans and Blowers. Düsseldorf, Germany. June 16–20, 2014. V01AT01A024. ASME.

[18] Balasubramanian, K., Turner, M. G., Siddappaji, K. "Novel Curvature-Based Airfoil Parameterization for Wind Turbine Application and Optimization." *ASME Turbo Expo 2017: Turbomachinery Technical Conference and Exposition* (pp. V009T49A020) (2017, June). American Society of Mechanical Engineers.

[19] Mahmood, S. M. H., Turner, M. G., Siddappaji, K. "Flow characteristics of an optimized axial compressor rotor using smooth design parameters." *ASME Turbo Expo 2016: Turbomachinery Technical Conference and Exposition* (V02CT45A018). American Society of Mechanical Engineers. (2016, June).